Thin plate manipulation by an under-actuated robotic soft gripper utilizing the environment

Toshihiro Nishimura, *Student Member, IEEE,* Kaori, Mizushima,
Yosuke Suzuki, *Member, IEEE,* Tokuo Tsuji, *Member, IEEE,* and Tetsuyou Watanabe, *Member, IEEE*

***Abstract*— This paper presents methodologies for dexterous manipulation by an underactuated robotic soft gripper with a low DOF. While the softness and passive joints provide a stable grasp, the manipulations become challenging owing to the complexities of modeling and state estimation. To investigate the drawbacks, target manipulations using a support surface and gravity are defined in this study. By realizing the target manipulations, methodologies for utilizing both the support surface and gravity in manipulation are validated. For manipulation utilizing the support surface, the key states—at which the type of gripper motion primitive changes—are defined, and gripper motion at the key states is produced with a DNN-based motion generator. For manipulation utilizing gravity, the fall risk of the object is formulated as a constraint for a criterion function, and a parameters-online-exploration based methodology is adopted. The validity of the methodologies is demonstrated through several experiments.**

I. Introduction

Softness is a key requirement for stable object grasp. Softness provides low contact impact, safe interaction with the object and environment, high friction, and adaptation to the object shape. Another key factor is utilization of an environment. Intentional contact with a table deforms the compliant elements, and shifting of the grasping mode is feasible. With a low DOF, multiple styles of grasping are obtained. With these aspects in mind, an under-actuated robotic soft gripper was developed [1] (see Fig. 1). A ratchet was installed at the under-actuated joint; the grasping mode is altered when the ratchet comes in contact with a supporting surface such as a table. Parallel gripper, pinching, and enveloping modes are available with only one actuator. The gripper has a soft surface, which is constructed from a deformable rubber bag filled with an incompressible fluid and a microgripper inside the fluid [2][3][4]. The microgripper increases the weight-carrying capacity of robotic hand. The grasping of a wide variety of objects was realized using the gripper.

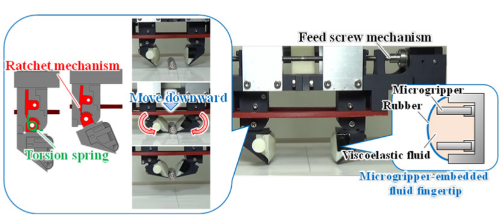

Figure 1. The under-actuated robotic soft gripper [1] whose grasping mode is altered by contact with a support surface

The next challenge is to manipulate an object using this gripper. The soft surfaces and passive joints of the soft gripper cause uncertainties in state estimation and complexities of modeling. These issues are common for soft robotic hands. Moreover, the gripper has only one actuator. Therefore, utilization of an environment is key for realizing dexterous manipulation. In this study, two types of utilizations of environment are considered. One is to utilize a support surface such as a table, and the other is to utilize gravity. A relevant example of manipulations incorporating both these utilizations is illustrated in Fig. 2. This is the target manipulation inspired by in-hand human manipulations utilizing the environments [5][6]. First, the gripper picks up the target, which is a thin object laid flat, in an imbalanced manner, wherein one finger is bent by a contact with the table while the other finger is not (*Initial grasp*). From the imbalanced grasping state, the object is brought to a standing position via reiterated up and down motions as well as closing and opening of the gripper (*Stand-up manipulation*). Lastly, the object is rotated by utilizing gravitational force such that the object is brought to the standing position in the longitudinal direction (*Rotation manipulation*). The operation is aimed at inserting the object into a box. By realizing the target manipulation, we will reveal the methodologies for utilizing both the support surface and gravity in manipulation via soft robotic hands with low DOF.

The main contributions of this study are manipulation strategies allowing 1) the uncertainties in state estimation and complexities of modeling, 2) only visual inputs to generate gripper motions, and 3) unexpected object motions, which are recovered by subsequent motions. At the stand-up manipulation, a learning-based approach utilizing human demonstration data (obtained from manual operations of the gripper) was adopted utilizing the concept of key states at which the type of motion primitive changed. A strategy for controlling the gripper at only the key states, was presented. By the concept, we developed the framework wherein the motion generation was repeated until the object attained the target posture. At the rotation manipulation, a parameters-online-exploration based approach was adopted, and unknown parameters were identified by repeated exploring motions until the object attained the target posture, while completely avoiding fall risk.

* Research partly supported by JSPS KAKENHI Grant Number 16H04298.
T. Nishimura and K. Mizushima are with the Graduated school of Natural science and Technology, Kanazawa University, Kakuma-machi, Kanazawa, 9201192 Japan (e-mail: to.nishimura@stu.kanazawa-u.ac.jp).

Y. Suzuki, T. Tsuji, and T. Watanabe are with the Faculty of Mechanical Engineering, Institute of Science and Engineering, Kanazawa University, Kakuma-machi, Kanazawa, 9201192 Japan (e-mail: te-watanabe@ieee.org)

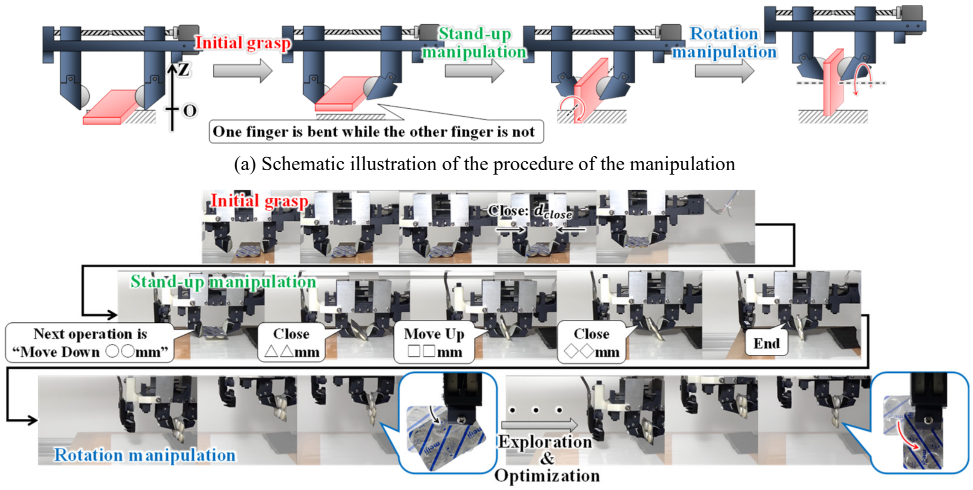

(a) Schematic illustration of the procedure of the manipulation

(b) Example of the generated manipulation

Figure 2. Target manipulation where a target sheet lying flat is picked up for insertion into a box. Initial grasp: the gripper picks up the target object in an imbalanced manner, wherein one finger is bent by a contact with the table, while the other finger is not. Stand-up manipulation: from the imbalanced grasping state, the object is made to stand-up via reiterated gripper motions of moving up and down, closing, and opening. Rotation manipulation: the object is rotated utilizing gravity such that the object stands up in the longitudinal direction.

A. Related works

A number of robotic hands have been developed [7]. Recently, softness has been attracting attention owing to its abovementioned benefits, and robotic hands with softness have been developed, e.g., ROBO hand [8][9], lightweight underactuated pneumatic fingers [10], ISR-SoftHand [11] and jamming gripper [12][13], Pisa-IIT Hand [14][15], and Velo Gripper [16]. A more detailed review is available in [1].

The softness in robotic hands enables high adaptation to target object and facilitates a stable grasp with a low DOF. However, the high adaptation renders it challenging to modify the grasped object’s pose and position. Manipulation using soft robotic hands is challenging. A solution is to use an environment that can be utilized as if it was another DOF. Object manipulation utilizing environments have been investigated [17][18][19][20]. Mason and Rodriguez et al. focused on pivoting manipulation utilizing support surfaces such as table [21][22][23]. Francisco et al. realized pivoting task utilizing gravity [24][25]. However, soft robotic hands were not the subject of these studies. The soft components renders it challenging to identify the parameters for the pivoting manipulation and to control the pivoting angle. It is necessary to develop a fresh strategy to address the uncertainties in the application of soft robotic hands.

Another approach to address the uncertainties or softness is the application of machine learning methodologies. Among these methodologies, DNN and Bayesian optimization, which are closely related to this study, are focused on. DNN is a highly effective tool to generate complex robot motions, and it has been used to develop a number of motion planners and generators [26][27][28][29][30]. However, soft robotic hands have been studies less. A. Gupta et al. [28] presented a guided policy search based algorithm to generate a manipulation-motion with the ROBO hand based on human demonstration data [8][9]. The generation of recovery motion and regrasping motion were not studied. The proposed methodology is based on multimodal integration learning method [26][29][30], wherein the autoencoder [31][32] was utilized to connect sequential robot motions, RGB images, and sound spectrums and to generate a robot motion from an image sequence. The main dissimilarity between this method and the proposed method is the sequence of data. In the latter, only the infrequent key states were considered to address an unexpected motion due to the softness and passivity of the newly developed gripper.

Bayesian optimization [33], [34] has been adopted for identifying optimal parameter values [35][36][37][38]. A few studies were focused on robotic hands [35]. Nogeira et al. defined an unsafe grasp as one wherein the grasp parameters are highly sensitive to marginal perturbations; they proposed a method for realizing a safe grasp. “Safe” in that study is dissimilar from “*safe*” aimed at in this study; the latter implies the avoidance of falling down. For this purpose, Safe Bayesian optimization [36][39], which was originally adopted for identifying control parameters for quadcopters, was adopted in this study.

To our knowledge, there is no study on the completion of complex manipulation by a soft robotic hand, using two types of machine learning based methodologies.

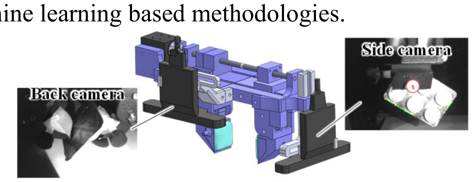

Figure 3. Position of cameras

II. SYSTEM FOR MANIPULATIONS

The developed under-actuated robotic soft gripper [1] is mounted on the XYZ motorized liner stage (Oriental motor). To obtain visual information of the object and gripper, two cameras (Intel RealSense SR300) were installed, one each at the back and side of the gripper, as illustrated in Fig. 3. The infrared image from the back camera was utilized during the initial grasp and stand-up manipulations, while the infrared image from the side camera was utilized during the rotation manipulation.

The target object is a thin and deformable rectangular object such as a PTP packaging sheet exhibited in Fig. 2(b). The size, shape, texture, gravitational center, and friction of the object are assumed to be unknown. A packing operation was considered, wherein such a thin object is inserted in a box. For the insertion, the study targeted a task, wherein the object is manipulated such that it stands up in the longitudinal direction from the initial lay-flat posture.

III. Strategies for Manipulations

A. Initial grasp

Human demonstration data was collected for the target manipulation, and the procedure for the manipulation was learned. The aim is to pick up the object, which is lying flat on the edge of the table, in an imbalanced manner wherein one finger is bent by a contact with the table, while the other finger is not. The amount of lateral movement is then determined such that the center position of the gripper coincides with the position of the table edge in the lateral direction. The amount of downward movement is determined by the lock position of the ratchet gear of the right finger. The closing distance is determined by the size of the target object, which can be estimated from a single image. Therefore, the problem is formulated as the derivation of the closing distance d_{close} ($\in \mathbb{R}$) from a single image captured by the back camera $\boldsymbol{u}_i \in \mathbb{R}^{45152}$($256 \times 192$ pixels). Here, the $\boldsymbol{u}_i$ when the right fingertip made contact with the table ($z = 0$ mm in Fig. 2(a)) was utilized.

The problem is resolved by learning the relationship between d_{close} and $\boldsymbol{u}_i$ from the human demonstration data. The autoencoder [31][32] and GRNN (Generalized Regression Neural Network) [40] were adopted, as illustrated in Fig. 4:

$$d_{\text{close}} = GRNN_{initial}(\boldsymbol{u}_{if}(\boldsymbol{u}_i)) \tag{1}$$

First, the image features $\boldsymbol{u}_{if}$ ($\in \mathbb{R}^{50}$)are extracted using the autoencoder. The autoencoder is a neural network comprising input, hidden, and output layers. Learning was conducted such that the input for the input layer equals the output for the output layer; moreover, it is an unsupervised learning. The layer structure is symmetric with respect to the hidden center layer. By utilizing a smaller number of neurons for the hidden center layer than the number of the input or the output, low-dimensionalized data can be obtained at the hidden center layer. This implies that the input is encoded to the low-dimensionalized data while the output is decoded from the low-dimensionalized data. Therefore, it is feasible for the hidden center layer to contain the low-dimensionalized image feature. By selecting only the encoder part, the function of extracting the low-dimensionalized image feature from the image can be constructed. The function is referred to as image feature extraction encoder (IFEE) in this study:

$$\boldsymbol{u}_{if} = IFEE(\boldsymbol{u}_i) \tag{2}$$

Next, the closing distance of the gripper d_{close} from $\boldsymbol{u}_{if}$ is derived using GRNN. GRNN was adopted in order to obtain various values of d_{close} according to $\boldsymbol{u}_i$. GRNN is constructed using a radial basis and special linear layers. For the available training data set ($\boldsymbol{u}_{if_1}, d_{\text{close}_1}$), ($\boldsymbol{u}_{if_2}, d_{\text{close}_2}$), $\cdots$, ($\boldsymbol{u}_{if_n}, d_{\text{close}_n}$), the output d_{close} for the input $\boldsymbol{u}_{if}$ is expressed as

$$d_{\text{close}} = \frac{\sum_{i=1}^{n} d_{\text{close}_i} \exp\left(-\left\|\boldsymbol{u}_{if} - \boldsymbol{u}_{if_i}\right\|^2 / (2\varepsilon^2)\right)}{\sum_{i=1}^{n} \exp\left(-\left\|\boldsymbol{u}_{if} - \boldsymbol{u}_{if_i}\right\|^2 / (2\varepsilon^2)\right)} \tag{3}$$

where ε is a constant parameter. It is noteworthy that for GRNN, a learning process is not required. If adequate number of data sets are available, a GRNN that approximates the relationship between $\boldsymbol{u}_{if}$ and d_{close} can be constructed.

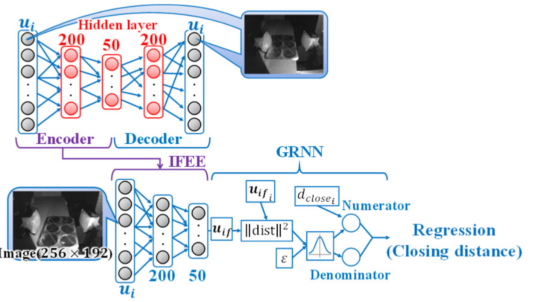

Figure 4. Neural network for deriving the closing distance of the gripper based on the image from the back camera at initial grasp

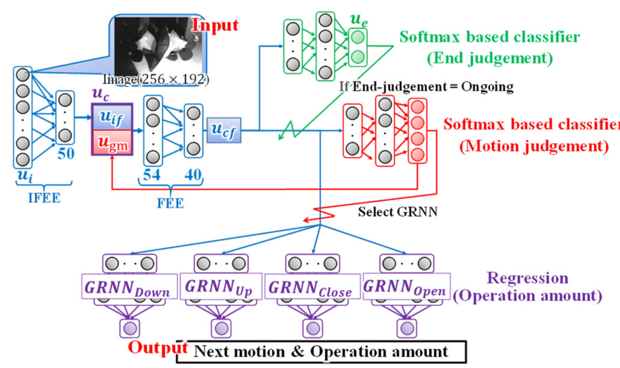

Figure 5. Motion generator for stand-up manipulation

B. Stand-up manipulation

We present a gripper motion generator whose input is the IR images of the back camera, based on the concept of the key state. In the case of the gripper, the key state is straightforwardly defined to be the state where the type of the gripper motion command changed. From the sequential data of images and gripper motion commands obtained from human demonstration, the data at the key states were selected. The only this selected data was utilized to learn the procedure for the complex manipulation, wherein the object is made to stand up via reiterated gripper motions. With this approach, the problem was simplified, and the number of learning targets was reduced substantially.

The problem is to develop a motion generator that repeatedly provides the gripper motion commands at the key states according to the image input such that the object finally attains the targeted standing posture.

The gripper motions were classified into four; moving down, moving up, closing the gripper, and opening the gripper.

$$\boldsymbol{u}_{\mathrm{gm}} = \left[\delta_{\mathrm{down}}, \delta_{\mathrm{up}}, \delta_{\mathrm{close}}, \delta_{\mathrm{open}}\right]^{\mathrm{T}} \quad (4)$$

$\boldsymbol{u}_{\mathrm{gm}}$ represents the classified gripper motion, where δ_{i} ($i \in \{down, up, close, open\}$) takes 1 or 0, and $\sum_{\mathrm{i}} \delta_{\mathrm{i}} = 1$. For example, the gripper-closing motion is expressed by $\boldsymbol{u}_{\mathrm{gm}} = [0,0,1,0]^{\mathrm{T}}$. $\sum_{\mathrm{i}} \delta_{\mathrm{i}} = 1$ implies that the gripper motion is limited to one of the four motions at a time; combinations of the motions were not considered. The key state is then defined as the state when $\boldsymbol{u}_{\mathrm{gm}}$ changed, namely, the commanded gripper motion was completed, and the subsequent command was communicated to the gripper. By controlling the gripper at only the key states, unexpected object motions can be addressed. According to the states of the object and gripper after the completion of motion, the subsequent motion is determined. If the object motion was an unexpected one, the subsequent motion could be a recovery motion. Therefore, the object attains the targeted posture notwithstanding whether the generated motions include unexpected ones, and robust manipulation to error in state estimation was obtained.

The motion generator was constructed mainly using feature extraction and the output layers, as illustrated in Fig. 5. To generate sequential motions, the generator utilized the IR image $\boldsymbol{u}_{\mathrm{i}}$ and the previous gripper motion type $\boldsymbol{u}_{\mathrm{gm}}$. By feedbacking the $\boldsymbol{u}_{\mathrm{gm}}$, the generated subsequent motion can be different from the previous one, and a recovery from an unexpected object state can be expected. Therefore, the features for the combination of the $\boldsymbol{u}_{\mathrm{gm}}$ and $\boldsymbol{u}_{\mathrm{i}}$ for the state resulting from the $\boldsymbol{u}_{\mathrm{gm}}$, were extracted. The dimensions of $\boldsymbol{u}_{\mathrm{gm}}$ and $\boldsymbol{u}_{\mathrm{i}}$ exhibit significantly high variations. Then, the features were extracted from the combination of $\boldsymbol{u}_{\mathrm{gm}}$ and $\boldsymbol{u}_{\mathrm{if}}$, which is the low-dimensionalized image feature expressed in equation (2):

$$\boldsymbol{u}_c = [\, \boldsymbol{u}_{if} \quad \boldsymbol{u}_{\mathrm{gm}} \,]^T \ (\in \mathbb{R}^{54}) \quad (5)$$

By utilizing the autoencoder, the feature vector $\boldsymbol{u}_{cf} \in \mathbb{R}^{40}$was derived:

$$\boldsymbol{u}_{cf} = FEE(\boldsymbol{u}_c) \quad (6)$$

where FEE (feature extraction encoder) denotes the encoder part of the autoencoder.

With the feature vector $\boldsymbol{u}_{cf}$, three types of networks were constructed for the three types of outputs. The first output (end judgment) network judged whether the object attained the final targeted posture. The softmax function was used for the network:

$$\delta_{end_i} = \frac{\exp\left(\boldsymbol{w}_i^T \boldsymbol{u}_{cf} + \gamma_i\right)}{\sum_j \exp\left(\boldsymbol{w}_j^T \boldsymbol{u}_{cf} + \gamma_j\right)} \quad (i = 1,2) \quad (7)$$

where $\boldsymbol{w}_i$ and γ_i are the network parameters, which are obtained through learning. One of the output neurons provides the probability of completion, while the other provides that of being ongoing. If the judgement was ongoing, then the second output (motion judgement) network was activated, and an appropriate type of subsequent gripper motion was determined according to the current states of the object and gripper. Considering the discreteness of the output $\boldsymbol{u}_{\mathrm{gm}}$, it was derived using softmax function. The operation amount for the selected gripper motion (indicated by the output $\boldsymbol{u}_{\mathrm{gm}}$) was derived at the last network. As a continuous value was to be derived, GRNN was utilized. Regression was conducted for each gripper motion type, and then, GRNN for each type (four GRNNs in total) was prepared. The GRNN whose corresponding component of the output $\boldsymbol{u}_{\mathrm{gm}}$ was 1 was selected, and the corresponding operation amount was derived. The overall network structure is illustrated in Fig. 5. A noteworthy feature of the gripper motion is that only type $\boldsymbol{u}_{\mathrm{gm}}$ was fed back, while its operation amount d_c was not.

The data for training $\mathcal{D}$ is expressed by

$$\mathcal{D} = \left[\boldsymbol{u}_i, \boldsymbol{u}_{\mathrm{e}}, \boldsymbol{u}_{\mathrm{gm}}, d_c\right]^T \quad (8)$$

where $\boldsymbol{u}_i$ is the image input captured by the back camera, $\boldsymbol{u}_{\mathrm{e}} = \left[\delta_{end_1}, \delta_{end_2}\right]^T$expresses whether the object attained the final posture ($[0, 1]^T$) or not ($[1, 0]^T$), $\boldsymbol{u}_{\mathrm{gm}}$ is the gripper motion type that provided the state $\boldsymbol{u}_i$, and d_c is its operation amount.

C. Rotation manipulation

Utilizing gravity, the object was rotated by 90° around the grasping points such that the object stands up in the longitudinal direction. The problem is to explore the optimal grasping points that provide rotation angle of 90°, avoiding falling down of the object. After the rotation, by making the object contact with the table, the object posture got to either the initial or desired one. Therefore, repeated exploring manipulations from the same initial object posture can be adopted, and a parameter-online-exploration based approach is preferable.

Here, the following manipulation was considered:

Step 1: The gripper was closed, and the target object was grasped and lifted up.

Step 2: The opening action of the gripper was continued until the object's rotation was detected. The opening action stopped when the rotation started. The rotation occurs owing to the moment resulting from the gravitational force and stops owing to contact friction.

In step 2, the opening action of the gripper could be continued until the rotation angle reached 90°. However, this method does not ensure that the rotation angle reaches 90° (or the angle close to 90°). On the other hand, different grasping points provide varying moment and rotation angles, as illustrated in Fig. 6. We then took the above way. Note that the rotation angle was derived from the image captured by the side camera.

Here, we consider the case illustrated in Fig. 6. Let θ be the rotation angle of the object, I_r be the moment of inertia at the rotational center, l_g be the length from the rotational center to the center of gravity, m_{o} be the mass of the object, g be the acceleration due to gravity, f_n be the normal component of the grasping force, μ_d be the coefficient of viscoelastic frictional moment, and μ_c be the coefficient of frictional moment. Then, the dynamics of the object is represented by [21]:

$$-I_r\ddot{\theta} + m_o g l_g \cos\theta = \mu_d\dot{\theta} + \mu_c f_n \tag{9}$$

The relationship appears convenient to apply. However, owing to the softness of the gripper and unevenness of the object surface, μ_d and μ_c are not constant:

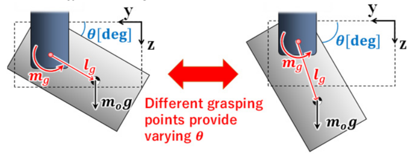

Figure 6. Mechanical relationship for the rotation manipulation

Algorithm 1: Safe Bayesian Optimization for the rotation manipulation	
Initial value & Definitions	Domain: A, Constants: b, β, σ_ω Lowest function value: $J_{min} = 0$
	Try the manipulation at $\boldsymbol{a}_1$, and observe the rotation angle $\theta(\boldsymbol{a}_1)$ and evaluate $\hat{J}(\theta(\boldsymbol{a}_1))$
For : n = 2,3,⋯	
	Update $\mu_n, \sigma_n, u_n, l_n$
	$S_n = \{\boldsymbol{a} \in A \mid l_n(\boldsymbol{a}) > 0\}$
	$M_n = \{\boldsymbol{a} \in S_n \mid u_n(\boldsymbol{a}) > \max_{\boldsymbol{a}' \in A} l_n(\boldsymbol{a}')\}$
	$g_n(\boldsymbol{a}) = \left\lvert\left\{\boldsymbol{a}' \in A \backslash S_n \middle\vert l_{n,(\boldsymbol{a},u_n(\boldsymbol{a}))}(\boldsymbol{a}') > J_{\min}\right\}\right\rvert$
	$G_n = \{\boldsymbol{a} \in S_n \mid g_n(\boldsymbol{a}) > 0\}$
	$\boldsymbol{a}_{n+1} = \underset{\boldsymbol{a} \in M_n \cup G_n}{\operatorname{argmax}}(u_n(\boldsymbol{a}) - l_n(\boldsymbol{a}))$
	Attempt the manipulation at $\boldsymbol{a}_{n+1}$, observe the rotation angle $\theta(\boldsymbol{a}_{n+1})$, and evaluate $\hat{J}(\theta(\boldsymbol{a}_{n+1}))$
End	

Figure 7. Algorithm of Safe Bayesian Optimization for exploring the grasping point maximizing function (Eq. (11)), which provides a rotation angle approximately equal to 90°, avoiding falling down of the object

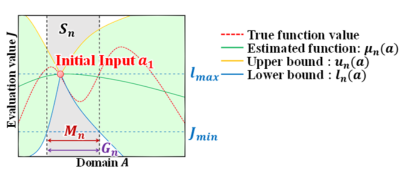

(a) Initial input $\boldsymbol{a}_1$: selected by visual information

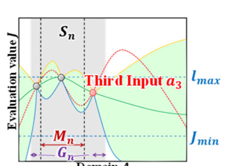

(b) Third input $\boldsymbol{a}_3$

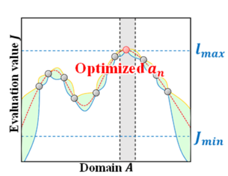

(c) Optimized input $\boldsymbol{a}_n$

Figure 8. Schematic illustration of Safe Bayesian Optimization

$$\mu_c = \mu_c(f_n, \theta, \boldsymbol{a}), \quad \mu_d = \mu_d(f_n, \theta, \boldsymbol{a}) \tag{10}$$

where $\boldsymbol{a}$ denotes the grasping points. It is challenging to derive an explicit equation (10). Therefore, instead of considering equation (10), the $\boldsymbol{a}$ providing $\theta = 90°$ is identified by manipulations through exploration. In order to avoid falling down, Safe Bayesian Optimization [36][39] was adopted. By describing the risk of falling down as a constraint for a criterion function, the manipulation with the exploration was repeated until the manipulation succeeded, completely circumventing the risk of falling down.

Bayesian optimization [33], [34] aims to obtain an input value that maximizes an unknown function through several explorations. Bayesian optimization uses a Gaussian process to approximate the function based on past observation values, and predicts the input, which is an optimal exploration target to maximize the function. By repeating exploration with the Bayesian optimization, the optimal input, which maximizes the function with a smaller number of the explorations than random trials, can be identified. In this study, the exploration domain was defined for the grasping points $\boldsymbol{a}$, and the rotation angle θ at the grasping points was utilized to construct the following criterion function:

$$J(\boldsymbol{a}) = J(\theta(\boldsymbol{a})) = 90 - |90 - \theta(\boldsymbol{a})| \tag{11}$$

The optimized grasping points $\boldsymbol{a}$, which maximize J and provide a rotation angle close to 90°, is obtained as follows: Let A be an exploration domain for the input vector $\boldsymbol{a}$ ($\in A$). The i th observation value is expressed by $\hat{J}(\boldsymbol{a}_i) = J(\boldsymbol{a}_i) + \sigma_\omega$ (with noise σ_ω (= 0.05 in the system in this study)), which is provided by the image from the side camera. After the nth observation, the Gaussian process estimates a function output for an arbitrary $\boldsymbol{a}$ with a form of Gaussian whose mean is $\mu_n(\boldsymbol{a})$ and variance is $\sigma_n^2(\boldsymbol{a})$:

$$\mu_n(\boldsymbol{a}) = \boldsymbol{k}_n(\boldsymbol{a})(\mathbf{K}_n + \mathbf{I}_n\sigma_\omega^2)^{-1}\hat{\boldsymbol{J}}_n \tag{12}$$

$$\sigma_n^2(\boldsymbol{a}) = k(\boldsymbol{a},\boldsymbol{a}) - \boldsymbol{k}_n(\boldsymbol{a})(\mathbf{K}_n + \mathbf{I}_n\sigma_\omega^2)^{-1}\boldsymbol{k}_n^{\mathrm{T}}(\boldsymbol{a}) \tag{13}$$

where k is the covariance function, $\boldsymbol{k}_n$ is the covariance vector, $\mathbf{K}_n$ is the kernel matrix, $\hat{\boldsymbol{J}}_n$ is the vector of the observed function values, and $\mathbf{I}_n$ is the identity matrix:

$$k(\boldsymbol{a}_i, \boldsymbol{a}_j) = \exp\left(-\left\|\boldsymbol{a}_i - \boldsymbol{a}_j\right\|^2/(2b^2)\right)$$

$$\boldsymbol{k}_n = [k(\boldsymbol{a},\boldsymbol{a}_1), \dots, k(\boldsymbol{a},\boldsymbol{a}_n))],$$

$$[\mathbf{K}_n]_{(i,j)} = k(\boldsymbol{a}_i, \boldsymbol{a}_j)$$

$$\hat{\boldsymbol{J}}_n = \left[\hat{J}(\boldsymbol{a}_1), \dots, \hat{J}(\boldsymbol{a}_n)\right]^{\mathrm{T}}$$

The upper and lower confidence bounds are expressed by

$$u_n(\boldsymbol{a}) = \mu_n(\boldsymbol{a}) + \beta\sigma_n(\boldsymbol{a}) \tag{14}$$

$$l_n(\boldsymbol{a}) = \mu_n(\boldsymbol{a}) - \beta\sigma_n(\boldsymbol{a}) \tag{15}$$

where $\beta > 0$ is the confidence interval. A larger β enhances the exploitation performance, while a smaller β enhances the exploration performance.

Safe Bayesian Optimization limits the exploration domain to the safe one and prevents the system state failures from being unsafe. Concretely, the set of the safe region S_n is expressed by

$$S_n = \{\boldsymbol{a} \in A \mid l_n(\boldsymbol{a}) > J_{min}\} \tag{16}$$

where J_{min} is the safe threshold for the function value $J(\boldsymbol{a})$. In this study, we set $J_{\min} = 0$ corresponding to no-rotation, which indicates falling down, and avoided the falling down event during the exploration. The subsequent exploration was conducted at

$$\boldsymbol{a}_{n+1} = \underset{\boldsymbol{a} \in M_n \cup G_n}{\operatorname{argmax}}(u_n(\boldsymbol{a}) - l_n(\boldsymbol{a})) \tag{17}$$

where M_n provides the high-probability bounds for maximizing the function on S_n, and G_n provides domains which are newly judged to be safe on S_n. The exploration procedure is illustrated in Fig. 7, and Fig. 8 illustrates the schematic of the procedure. Note that $l_{n,(\boldsymbol{a},u_n(\boldsymbol{a}))}$ is the lower confidence bound calculated using equation (15) based on past data and data that is artificially constructed by the input of $\boldsymbol{a}$ and output of $u_n(\boldsymbol{a})$.

As the target is a rectangular object and as the gripper is used (see Fig. 9), the y and z coordinate values form the exploration target and are identical for both the fingertips. Then, the dimension of the exploration domain was two, and the grasping points are expressed as $\boldsymbol{a} = [y, z]$. It is noteworthy that the domain included only the upper area, where it was feasible for the gripper to make contact, as illustrated in Fig. 9. It was not feasible for the gripper to make contact with the lower area owing to the presence of the fingernail.

In actual situations, the initial grasping points are to be deliberately selected, and for preventing falling down, they are not to be the gravitational center. Based on the image from the side camera, which is exhibited in Fig. 10, the initial grasping points $\boldsymbol{a}_1$ was determined by

$$\boldsymbol{a}_1 = [y_c + (m - 1.5)l_m, z_c] \tag{18}$$

where

$$m = \underset{m\in\{1,2\}}{\mathrm{argmax}}|l_m| \tag{19}$$

The other notations are exhibited in Fig. 10.

Additionally, for $\theta \neq 90°$, a contact between the object and the table could provide $\theta = 90°$ if θ was in the proximity of 90°. Although the explored input in this case was not optimal, the targeted posture was obtained. In this case, we finished the manipulation by judging that the manipulation was completed. The overall procedure is illustrated in Fig. 11.

IV. EXPERIMENTAL VALIDATIONS

A. *Initial grasp and stand-up manipulation*

Here, both the initial grasp and stand-up manipulation were evaluated simultaneously. The objects during the training were PTP packaging sheet (No. 1 in Fig. 12), the sheets painted with the four patterns (Nos. 2–5), and the cut half sheet (No. 6). The test objects were the sheet with a dissimilar pattern (No. 7 in Fig. 12), tablet pillbox (No. 8), another PTP packaging sheet (No. 9), and business card (No. 10). Table I presents the number of training data for the stand-up manipulation. While constructing $\boldsymbol{u}_{\mathrm{e}}$, the labels *Down*, *Up*, *Close*, and *Open* were treated as *Ongoing*. The parameter $\varepsilon = 0.3$ was set for all GRNNs by adopting grid search to the training data. Table II presents the results. Both the types of manipulation were successful for all the trained and test objects except for the card. The failure of the manipulation was due to the card's substantially low thickness, which caused the misjudgment of completion (Fig. 13). An example of recovery motions can be observed in the attached video, wherein additional opening and closing motions were implemented to obtain an expected object state from an unexpected object state, which had resulted from wrong motion due to wrong state estimation. In total, five recovery motions were observed at all the examinations. The small number of training data was also one of the features of this methodology (Table I). The total number of training data was 1173, as can be observed in Table I. The number of image frames for each manipulation was an average of 600 (= 30 s × 20 fps). Of the entire data (1173 / (600 × 15)), 13 % is required; this validated that the proposed methodology simplified the problem.

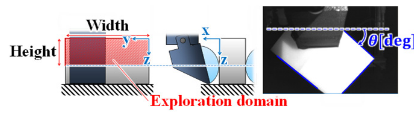

Figure 9. The exploration domain and the rotation angle

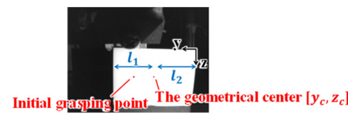

Figure 10. Initial grasping points

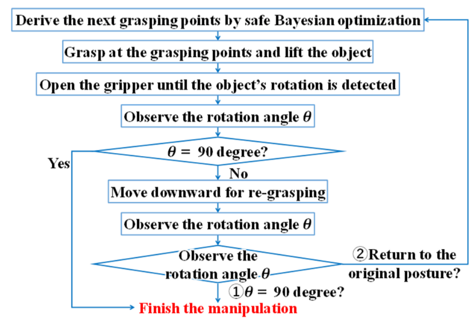

Figure 11. Procedure for the rotation manipulation

TABLE I. NUMBER OF TRAINING DATA FOR THE STAND-UP MANIPULATION

Label	Down	Up	Close	Open	End
Number of data	352	223	478	120	166

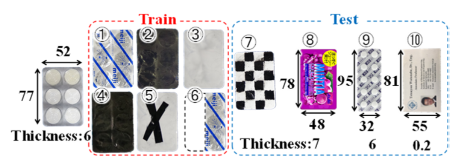

Figure 12. Target objects for the experimental evaluation of the initial grasp and the stand-up manipulation. The objects from No. 1 to 6 were for training while the other objects were for testing.

TABLE II. SUCCESS RATE OF INITIAL GRASP AND STAND-UP MANIPULATION

	Trained					Test				
Object number	1	2	3	4	5	6	7	8	9	10
Success rate	3/3	3/3	3/3	3/3	3/3	3/3	3/3	3/3	3/3	1/3

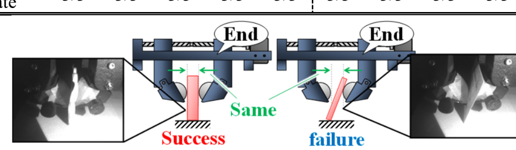

Figure 13. Successful grasping of the PTP packaging sheet and the failure of grasping of the thin business card

B. *Rotation manipulation*

The methodology was evaluated using the box with six pockets (70 × 50 × 16.5 mm, 18.8 g), which is illustrated in Fig. 14. The gravitational center was altered by placing a weight (5g) in one of the pocket. The exploration domain was

$$A = \left\{ \boldsymbol{a} = [y, z] \middle| \begin{matrix} 0 \le y \le 70 \\ 0 \le z \le 30 \end{matrix} \right\} \tag{20}$$

The interval for the exploration was 2.0 mm for each axis. The manipulation was completed when $|\mathrm{J} - 90| < 5$. The parameter $b = 7.07$ in the covariance function and $\beta = 60$ in the confidence bounds were set by adopting grid search at the practice phase utilizing the PTP sheet (No. 1 in Fig. 12).

The results when the weight was in pocket 2 are summarized in Table III and Fig. 15. Table IV presents the results with the weight placed in each of the six pockets, one pocket at a time. It is observed that the methodology worked effectively. It is noteworthy that there was no falling during any of the exploration manipulations.

C. Combination of all manipulations

The overall manipulation was conducted by combining the three manipulations. The corresponding result for the table pillbox is presented in Fig. 16. Table V presents the results for the four objects. It is observed that the combined manipulation was successful for all the objects except for the business card. The reason for the failure was similar to those presented in Table II. It is noteworthy that the success rate of rotation manipulation for the business card was 3/3. The attached video displays the successful combined manipulation of several objects.

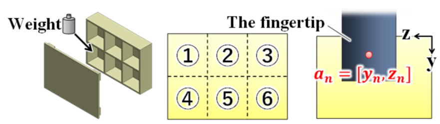

Figure 14. The target object for evaluating the rotation manipulation: a box with six pockets for varying the gravitational center.

TABLE III. THE OBTAINED PROCESS RESULTS WHEN THE WEIGHT WAS IN POCKET 2

	$n =$	1	2	3	4	5	6
$\boldsymbol{a}_n$	y_n [mm]	52	60	60	50	44	58
	z_n [mm]	24	30	18	30	14	24
	J_n	78.0	73.8	59.7	39.0	21.3	86.8

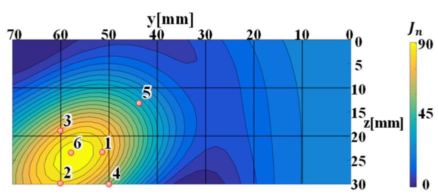

Figure 15. The explored grasping points and the corresponding criterion function values when the weight was in pocket 2

TABLE IV. RESULTS OF THE CASES WITH THE WEIGHT IN EACH OF THE SIX POCKETS, ONE AT A TIME.

Weight position [No]	Trial number	Success or not	Number of trial	Optimized grasping points y_n[mm]	Optimized grasping points z_n[mm]
1	1st	Success	2	60	28
	2nd	Success	6	58	26
	3rd	Success	2	60	28
2	1st	Success	6	58	24
	2nd	Success	6	56	24
	3rd	Success	7	58	24
3	1st	Success	1	52	24
	2nd	Success	1	52	24
	3rd	Success	1	52	24
4	1st	Success	2	62	30
	2nd	Success	2	62	28
	3rd	Success	2	62	38
5	1st	Success	4	48	30
	2nd	Success	6	62	28
	3rd	Success	8	52	30
6	1st	Success	3	62	30
	2nd	Success	2	62	26
	3rd	Success	2	60	28

Tablet pill box			
Initial grasp	Closing distance [mm]		9.6
Stand-up manipulation	Operation number	Motion	Operation amount [mm]
	1st	Down	16.20
	2nd	Close	8.30
	3rd	Up	11.65
	4th	Close	4.27
Rotation manipulation		J_n	$\boldsymbol{a}_n = [y_n, z_n]$
	1st	40	[58,24]
	2nd	32	[52,18]
	3rd	70	[52,30]
	4th	82	[42,26]

Figure 16. The result of the combined manipulation for the tablet pill box

TABLE V. SUCCESS RATE OF THE COMBINED MANIPULATION

	PTP packaging sheet (No. 1)	Tablet pillbox (No. 8)	PTP packaging sheet (No. 9)	Business card (No. 10)
Success rate	3/3	3/3	3/3	1/3

V. CONCLUSION

This study presented novel methodologies for dexterous manipulation (Fig. 2) using under-actuated robotic soft gripper with a low DOF developed previously by the authors (Fig. 1). In order to achieve dexterous manipulation, the utilization of an environment is key. The target manipulations utilizing a support surface and gravity were defined. Through realization of the target manipulations, the methodologies for utilizing the support surface and gravity in manipulation by a soft robotic hand were revealed. In order to deal with the softness and passivity of the gripper in the target manipulation utilizing the support surface, the key states where the type of gripper motion primitive changed were focused on, and a strategy for controlling the gripper at only the key states by using a DNN based motion generator, was presented. The motion generator was highly robust, and it was capable of addressing unexpected object motion and generating recovery motion. In the manipulation utilizing gravity, a parameters-online-exploration based approach was adopted to prevent falling down of the object. By formulating the fall risk as a constraint for a criterion function, the manipulation with exploration was repeated until the manipulation was successful, completely avoiding the fall risk. All the methodologies were combined, and the effectiveness of the obtained methodologies was demonstrated by experimentation.

The targeted manipulation was set considering the feasibility of conducting complex manipulations by using soft robotic hands with a low DOF, such as the soft gripper developed previously by the authors, and whether it is feasible to realize its atomization. The strategy of the approach based on key state could be adopted to various manipulations by other soft robotic hands, with appropriately defining the key states. Challenges in other complex manipulations and adaptation of the approach investigated in this study to other robotic systems are planned to be explored in future studies by the authors. Moreover, the authors intend to extend the set of available object types through their future studies, including the business card, whose manipulation was not completely successful in this study.

REFERENCE

[1] T. Nishimura, K. Mizushima, Y. Suzuki, T. Tsuji, and T. Watanabe, “Variable-grasping-mode underactuated soft gripper with environmental contact-based operation,” *IEEE Robot. Autom. Lett.*, pp. 1–1, 2017.

[2] R. Maruyama, T. Watanabe, and M. Uchida, “Delicate grasping by robotic gripper with incompressible fluid-based deformable fingertips,” in *Proc. 2013 IEEE/RSJ Int. Conf. on Intell. Robots Syst.*, 2013, pp. 5469–5474.

[3] R. Adachi, Y. Fujihira, and T. Watanabe, “Identification of danger state for grasping delicate tofu with fingertips containing viscoelastic fluid,” in *Proc. 2015 IEEE/RSJ Int. Conf. on Intell. Robots Syst.*, 2015, pp. 497–503.

[4] T. Nishimura, Y. Fujihira, R. Adachi, and T. Watanabe, “New Condition for Tofu Stable Grasping with Fluid Fingertips,” in *Proc. 2016 IEEE Int. Conf. on Autom. Sci. Eng.*, 2016, pp. 335-341.

[5] J. M. Elliott and K. J. Connolly, “A CLASSIFICATION OF MANIPULATIVE HAND MOVEMENTS,” *Dev. Med. Child Neurol.*, vol. 26, no. 3, pp. 283–296, Nov. 2008.

[6] I. M. Bullock, R. R. Ma, and A. M. Dollar, “A Hand-Centric Classification of Human and Robot Dexterous Manipulation,” *IEEE Trans. Haptics*, vol. 6, no. 2, pp. 129–144, Apr. 2013.

[7] M. Controzzi, C. Cipriani, and M. C. Carrozza, “Design of Artificial Hands: A Review,” 2014, pp. 219–246.

[8] R. Deimel and O. Brock, “A compliant hand based on a novel pneumatic actuator,” in *Proc. 2013 IEEE Int. Conf. on Robot. Autom.*, 2013, pp. 2047–2053.

[9] R. Deimel and O. Brock, “A novel type of compliant and underactuated robotic hand for dexterous grasping,” *Int. J. Rob. Res.*, vol. 35, no. 1–3, pp. 161–185, Jan. 2016.

[10] A. Dameitry and H. Tsukagoshi, “Lightweight Underactuated Pneumatic Fingers Capable of Grasping Various Objects,” in *Proc. 2016 IEEE Int. Conf. on Robot. Autom.*, 2016, pp. 2009–2014.

[11] M. Tavakoli and A. T. de Almeida, “Adaptive under-actuated anthropomorphic hand: ISR-SoftHand,” in *Proc. 2014 IEEE/RSJ Int. Conf. on Intell. Robots Syst.*, 2014, pp. 1629–1634.

[12] E. Brown, N. Rodenberg, J. Amend, A. Mozeika, E. Steltz, M. R. Zakin, H. Lipson, and H. M. Jaeger, “Universal robotic gripper based on the jamming of granular material,” *Proc. Natl. Acad. Sci.*, vol. 107, no. 44, pp. 18809–18814, Nov. 2010.

[13] J. R. Amend, E. Brown, N. Rodenberg, H. M. Jaeger, and H. Lipson, “A Positive Pressure Universal Gripper Based on the Jamming of Granular Material,” *IEEE Trans. Robot.*, vol. 28, no. 2, pp. 341–350, Apr. 2012.

[14] M. G. Catalano, G. Grioli, E. Farnioli, A. Serio, C. Piazza, and A. Bicchi, “Adaptive synergies for the design and control of the Pisa/IIT SoftHand,” *Int. J. Rob. Res.*, vol. 33, no. 5, pp. 768–782, Apr. 2014.

[15] G. Grioli, M. Catalano, E. Silvestro, S. Tono, and A. Bicchi, “Adaptive synergies: An approach to the design of under-actuated robotic hands,” in *Proc. 2012 IEEE Int. Conf. Intell. Robot. Syst.*, 2012, pp. 1251–1256.

[16] M. Ciocarlie, F. M. Hicks, R. Holmberg, J. Hawke, M. Schlicht, J. Gee, S. Stanford, and R. Bahadur, “The Velo gripper: A versatile single-actuator design for enveloping, parallel and fingertip grasps,” *Int. J. Rob. Res.*, vol. 33, no. 5, pp. 753–767, Apr. 2014.

[17] J. C. Trinkle and R. P. Paul, “Planning for Dexterous Manipulation with Sliding Contacts,” *Int. J. Rob. Res.*, vol. 9, no. 3, pp. 24–48, 1990.

[18] C. Eppner, R. Deimel, J. Álvarez-Ruiz, M. Maertens, and O. Brock, “Exploitation of environmental constraints in human and robotic grasping,” *Int. J. Rob. Res.*, vol. 34, no. 7, pp. 1021–1038, Jun. 2015.

[19] Y. Aiyama, M. Inaba, and H. Inoue, “Pivoting: A New Method of Graspless Manipulation of Object by Robot Fingers,” in *Proc. 1993 IEEE/RSJ Int. Conf. Intell. Robot. Syst.*, 1993, pp. 136–143.

[20] P. Tournassoud, T. Lozano-Perez, and E. Mazer, “Regrasping,” in *Proceedings. 1987 IEEE Int. Conf. on Robot. Autom.*, 1987, vol. 4, pp. 1924–1928.

[21] A. Holladay, R. Paolini, and M. T. Mason, “A general framework for open-loop pivoting,” in *Proc. 2015 IEEE Int. Conf. on Robot. Autom.*, 2015, pp. 3675–3681.

[22] N. Chavan-Dafle and A. Rodriguez, “Prehensile pushing: In-hand manipulation with push-primitives,” in *Proc. 2015 IEEE Int. Conf. Intell. Robot. Syst.*, 2015, pp. 6215–6222.

[23] N. C. Dafle, A. Rodriguez, R. Paolini, B. Tang, S. S. Srinivasa, M. Erdmann, M. T. Mason, I. Lundberg, H. Staab, and T. Fuhlbrigge, “Extrinsic dexterity: In-hand manipulation with external forces,” in *Proc. 2014 IEEE Int. Conf. on Robot. Autom.*, 2014, pp. 1578–1585.

[24] F. E. Vina B., Y. Karayiannidis, C. Smith, and D. Kragic, “Adaptive control for pivoting with visual and tactile feedback,” in *Proc. 2016 IEEE Int. Conf. on Robot. Autom.*, 2016, pp. 399–406.

[25] F. E. Vina B., Y. Karayiannidis, K. Pauwels, C. Smith, and D. Kragic, “In-hand manipulation using gravity and controlled slip,” in *Proc. 2015 IEEE/RSJ Int. Conf. on Intell. Robots Syst.*, 2015, pp. 5636–5641.

[26] K. Noda, H. Arie, Y. Suga, and T. Ogata, “Multimodal integration learning of robot behavior using deep neural networks,” *Rob. Auton. Syst.*, vol. 62, no. 6, pp. 721–736, Jun. 2014.

[27] S. Levine, P. Pastor, A. Krizhevsky, and D. Quillen, “Learning Hand-Eye Coordination for Robotic Grasping with Large-Scale Data Collection,” in *Proc. .Int. Sympo. on Exp. Robot.*, 2017, pp. 173–184.

[28] A. Gupta, C. Eppner, S. Levine, and P. Abbeel, “Learning dexterous manipulation for a soft robotic hand from human demonstrations,” in *Proc. 2016 IEEE/RSJ Int. Conf. on Intell. Robots Syst.*, 2016, pp. 3786–3793.

[29] C. Finn, Xin Yu Tan, Yan Duan, T. Darrell, S. Levine, and P. Abbeel, “Deep spatial autoencoders for visuomotor learning,” in *Proc. 2016 IEEE Int. Conf. on Robot. Autom.*, 2016, pp. 512–519.

[30] X. Yin and Q. Chen, “Deep metric learning autoencoder for nonlinear temporal alignment of human motion,” in *Proc. 2016 IEEE Int. Conf. on Robot. Autom.*, 2016, no. 1, pp. 2160–2166.

[31] M. F. Møller, “A scaled conjugate gradient algorithm for fast supervised learning,” *Neural Networks*, vol. 6, no. 4, pp. 525–533, Jan. 1993.

[32] B. A. Olshausen and D. J. Field, “Sparse coding with an overcomplete basis set: A strategy employed by V1?,” *Vision Res.*, vol. 37, no. 23, pp. 3311–3325, Dec. 1997.

[33] D. R. Jones, M. Schonlau, and W. J. Welch, “Efficient Global Optimization of Expensive Black-Box Functions,” *J. Glob. Optim.*, vol. 13, no. 4, pp. 455–492, 1998.

[34] E. Brochu, V. M. Cora, and N. De Freitas, “A tutorial on Bayesian optimization of expensive cost functions, with application to active user modeling and hierarchical reinforcement learning,” *ArXiv*, p. 49, 2010.

[35] J. Nogueira, R. Martinez-Cantin, A. Bernardino, and L. Jamone, “Unscented Bayesian optimization for safe robot grasping,” in *Proc. 2016 IEEE/RSJ Int. Conf. on Intell. Robots Syst.*, 2016, pp. 1967–1972.

[36] F. Berkenkamp, A. P. Schoellig, and A. Krause, “Safe controller optimization for quadrotors with Gaussian processes,” in *Proc. 2016 IEEE Int. Conf. on Robot. Autom.*, 2016, pp. 491–496.

[37] S. Bai, J. Wang, F. Chen, and B. Englot, “Information-theoretic exploration with Bayesian optimization,” in *Proc. 2016 IEEE/RSJ Int. Conf. on Intell. Robots Syst.*, 2016, pp. 1816–1822.

[38] O. Andersson, M. Wzorek, P. Rudol, and P. Doherty, “Model-predictive control with stochastic collision avoidance using Bayesian policy optimization,” in *Proc. 2016 IEEE Int. Conf. on Robot. Autom.*, 2016, pp. 4597–4604.

[39] Y. Sui, A. Gotovos, J. Burdick, and A. Krause, “Safe Exploration for Optimization with Gaussian Processes,” *Proc. 32nd Int. Conf. Mach. Learn.*, vol. 37, pp. 997–1005, 2015.

[40] Philip D. Wasserman, *Advanced Methods in Neural Computing*. 1993.